

Banner appropriate to article type will appear here in typeset article

Emergent rheotaxis of shape-changing swimmers in Poiseuille flow

B. J. Walker^{1†}, K. Ishimoto², C. Moreau², E. A. Gaffney³, M. P. Dalwadi¹

¹Department of Mathematics, University College London, London, WC1H 0AY, UK

²Research Institute for Mathematical Sciences, Kyoto University, Kyoto, 606-8502, Japan

³Wolfson Centre for Mathematical Biology, Mathematical Institute, University of Oxford, Oxford, OX2 6GG, UK

(Received xx; revised xx; accepted xx)

A simple model for the motion of shape-changing swimmers in Poiseuille flow was recently proposed and numerically explored by Omori *et al.* (2022). These explorations hinted that a small number of interacting mechanics can drive long-time behaviours in this model, cast in the context of the well-studied alga *Chlamydomonas* and its rheotactic behaviours in such flows. Here, we explore this model analytically via a multiple-scale asymptotic analysis, seeking to formally identify the causal factors that shape the behaviour of these swimmers in Poiseuille flow. By capturing the evolution of a Hamiltonian-like quantity, we reveal the origins of the long-term drift in a single swimmer-dependent constant, whose sign determines the eventual behaviour of the swimmer. This constant captures the nonlinear interaction between the oscillatory speed and effective hydrodynamic shape of deforming swimmers, driving drift either towards or away from rheotaxis.

1. Introduction

The behaviours of microswimmers in flows have long been a topic of broad theoretical and experimental study. Recently, Omori *et al.* (2022) numerically explored a model of a shape-changing swimmer in Poiseuille flow, posed in the context of the alga *Chlamydomonas* for comparison with their experimental findings. Their investigations suggested an interesting and subtle connection between the long-time behaviours of the microswimmer and the details of its changing speed and shape, with certain conditions apparently necessary for long-time upstream-facing swimming in the flow, referred to as *rheotaxis* by Omori *et al.*. Their ordinary differential equation (ODE) model may be simply stated in terms of a transverse coordinate y and the swimmer orientation θ as

$$\frac{dy}{dt} = \omega u(\omega t) \sin \theta, \quad (1.1a)$$

$$\frac{d\theta}{dt} = \gamma y(1 - B(\omega t) \cos 2\theta), \quad (1.1b)$$

† Email address for correspondence: benjamin.walker@ucl.ac.uk

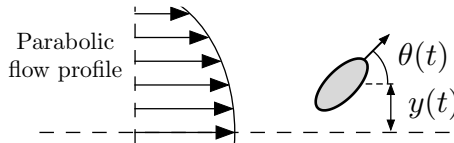


Figure 1: Notation and set-up. We illustrate a model swimmer in Poiseuille flow, located at a transverse displacement y from the midline of the parabolic flow profile. The swimming direction θ is measured from the midline, with $\theta = 0$ corresponding to downstream swimming.

with given initial conditions and with reference to the setup of fig. 1, where all quantities are considered dimensionless. We refer the interested reader to the work of Omori *et al.* (2022) for a full derivation of the model. The functions u and B capture the time-dependent active swimming speed and shape-capturing Bretherton constant (Bretherton 1962), respectively. These prescribed functions are assumed to be oscillatory with a shared high frequency $\omega \gg 1$. In particular, the swimming speed naturally scales with ω in eq. (1.1a), as the Stokes equations are both linear and independent of time except via boundary conditions (Kim & Karrila 2005). However, such a velocity scaling is absent from the explicitly stated equations of Omori *et al.* (2022), although it is present in their explored parameter regimes. The equations of Stokes flow are appropriate in the low-Reynolds-number and low-frequency-Reynolds-number regimes associated with many microswimmers, including *Chlamydomonas* (Guasto *et al.* 2012), and we will restrict our analysis to such regimes of practical interest. Here, γ is a fixed characteristic shear rate of the flow, non-negative without loss of generality. This model neglects any interactions of the swimmer with solid boundaries typically associated with Poiseuille flow, and we will proceed without additional consideration of boundary effects.

Via the numerical explorations of Omori *et al.* (2022), this model is noted to give rise to a range of complex, long-time behaviours, perhaps most remarkable of which is conditional convergence towards a central upstream-facing configuration. In this study, we will aim to analytically uncover the driving factors behind these long-time dynamics. Via a multiple-scale asymptotic analysis (Bender & Orszag 1999), as recently applied to similar models of swimming (Gaffney *et al.* 2022; Ma *et al.* 2022; Walker *et al.* 2022), we will show how the effective swimmer behaviour can be captured by a Hamiltonian-like quantity, whose slow evolution accurately encodes the long-time trends of behaviour noted by Omori *et al.* (2022). Further, we will identify a markedly simple relation between the eventual behaviour of the swimmer and its oscillating speed and shape, enabling the deduction of long-time dynamics through the calculation of a single swimmer-dependent constant.

2. Direct asymptotic analysis

The timescales present in the model of Omori *et al.* (2022) are best identified through a change of variable. Defining $z(t) := y(t)/\omega^{1/2}$, the system reads

$$\frac{dz}{dt} = \omega^{1/2} u(\omega t) \sin \theta, \quad (2.1a)$$

$$\frac{d\theta}{dt} = \gamma \omega^{1/2} z (1 - B(\omega t) \cos 2\theta). \quad (2.1b)$$

This suggests a natural fast timescale $T := \omega t$, that of the oscillating swimmer speed and shape. Additionally, $O(1)$ oscillations of u and B in eq. (2.1) drive $O(1)$ changes in z and θ over an intermediate timescale of $t = O(\omega^{-1/2})$. We will later see that these changes correspond to quasiperiodic orbits of the swimmer in the flow, quantifying motion on this timescale via $\tau := \omega^{1/2}t$. In addition to the two timescales T and τ evident from this system of equations, Omori *et al.* (2022) observed behavioural changes over longer timescales, with $t = O(1)$. Hence, we expect the system to evolve on three separated timescales, corresponding to T , τ , and t each being $O(1)$. Our overarching aim is to characterise and understand the behaviours of the system over the timescale $t = O(1)$.

To this end, we implement a multiple-scale analysis and formally write $z(t) = z(T, \tau, t)$ and $\theta(t) = \theta(T, \tau, t)$, treating each time variable as independent (Bender & Orszag 1999). This transforms the proper time derivative via

$$\frac{d}{dt} \mapsto \omega \frac{\partial}{\partial T} + \omega^{1/2} \frac{\partial}{\partial \tau} + \frac{\partial}{\partial t}, \quad (2.2)$$

which transforms eq. (2.1) into the system of partial differential equations (PDEs)

$$\omega z_T + \omega^{1/2} z_\tau + z_t = \omega^{1/2} u(T) \sin \theta, \quad (2.3a)$$

$$\omega \theta_T + \omega^{1/2} \theta_\tau + \theta_t = \omega^{1/2} \gamma z (1 - B(T) \cos 2\theta). \quad (2.3b)$$

Here and hereafter, subscripts of t , τ , and T denote partial derivatives. We will later remove the extra degrees of freedom that we have introduced by imposing periodicity of the dynamics in the intermediate and fast variables τ and T . Expanding z and θ in powers of $\omega^{-1/2}$ as $z \sim z_0 + \omega^{-1/2} z_1 + \omega^{-1} z_2 + \dots$ and $\theta \sim \theta_0 + \omega^{-1/2} \theta_1 + \omega^{-1} \theta_2 + \dots$, we obtain the $O(\omega)$ balance

$$z_{0T} = 0, \quad \theta_{0T} = 0, \quad (2.4)$$

so that $z_0 = z_0(\tau, t)$ and $\theta_0 = \theta_0(\tau, t)$ are independent of T . To determine how z_0 and θ_0 depend on τ and t , we must proceed to higher asymptotic orders.

We next consider the balance of $O(\omega^{1/2})$ terms in eq. (2.3), which reads

$$z_{1T} + z_{0\tau} = u(T) \sin \theta_0, \quad (2.5a)$$

$$\theta_{1T} + \theta_{0\tau} = \gamma z_0 (1 - B(T) \cos 2\theta_0). \quad (2.5b)$$

The Fredholm solvability condition for eq. (2.5) is equivalent to averaging over a period in T and enforcing T -periodicity of z_1 and θ_1 . Introducing the averaging operator $\langle \cdot \rangle$, defined via its action on functions $v(T, \tau, t)$ via

$$\langle v \rangle(\tau, t) := \int_0^1 v(T, \tau, t) dT, \quad (2.6)$$

we obtain the averaged equations

$$z_{0\tau} = \langle u \rangle \sin \theta_0, \quad (2.7a)$$

$$\theta_{0\tau} = \gamma z_0 (1 - \langle B \rangle \cos 2\theta_0), \quad (2.7b)$$

where $\langle u \rangle$ and $\langle B \rangle$ are the averages of $u(T)$ and $B(T)$, respectively, representing the average speed and shape of the model swimmer. In particular, $\langle u \rangle$ and $\langle B \rangle$ are constant, with the dynamics being rendered trivial if $\langle u \rangle = 0$; we exclude this case from our analysis and henceforth take $\langle u \rangle > 0$ without further loss of

generality[†]. We will also assume that $|\langle B \rangle| < 1$, which imposes only a minimal restriction on the admissible swimmer shapes, since $|B| \geq 1$ is typically associated with objects of exceedingly large aspect ratio (Bretherton 1962).

Of particular note, if viewed as a system of ODEs in τ , the system of eq. (2.7) corresponds precisely to the original dynamical system of eq. (2.1), suitably scaled, but with the time-varying speed and shape parameters replaced by their averages. We will shortly return to these equations and explore the ramifications of this observation in detail, in particular noting the existence of a Hamiltonian-like quantity, but first complete our analysis of the $O(\omega^{1/2})$ problem to determine the form of z_1 and θ_1 for later convenience.

Without solving eq. (2.7), we can deduce the form of z_1 and θ_1 by substituting eq. (2.7) into eq. (2.5), yielding the simplified system

$$z_{1T} = [u(T) - \langle u \rangle] \sin \theta_0, \quad (2.8a)$$

$$\theta_{1T} = -\gamma z_0 [B(T) - \langle B \rangle] \cos 2\theta_0. \quad (2.8b)$$

Integrating eq. (2.8) in T , recalling that z_0 and θ_0 are independent of T , yields the solution

$$z_1 = I_u(T) \sin \theta_0 + \bar{z}_1(\tau, t), \quad (2.9a)$$

$$\theta_1 = -\gamma z_0 I_B(T) \cos 2\theta_0 + \bar{\theta}_1(\tau, t), \quad (2.9b)$$

where \bar{z}_1 and $\bar{\theta}_1$ are functions of τ and t , undetermined at this order, and we define

$$I_u(T) := \int_0^T [u(\tilde{T}) - \langle u \rangle] d\tilde{T}, \quad I_B(T) := \int_0^T [B(\tilde{T}) - \langle B \rangle] d\tilde{T}. \quad (2.10)$$

Noting that $I_u(T)$ and $I_B(T)$ are T -periodic with period one, it follows that z_1 and θ_1 are T -periodic with the same period.

In principle, one could proceed to the next asymptotic order to determine how z_0 and θ_0 evolve in t through the derivation of an additional solvability condition. However, here, this procedure would be complicated by the absence of an explicit solution to the nonlinear system of eq. (2.7), compounded by the potentially t -dependent period of the solution, which would require using the generalised method of Kuzmak (1959). To circumvent this difficulty, we instead turn our attention back to eq. (2.7), seeking further understanding of the leading-order dynamics over the intermediate timescale τ .

3. A Hamiltonian-like quantity

If treated as a system of ODEs, we noted that eq. (2.7) closely resembles the original swimming problem, with averages taking the place of oscillatory swimming speeds and swimmer shapes. In fact, the equivalent ODE problem has been extensively studied, with Zöttl & Stark (2013) thoroughly exploring this dynamical system and identifying a Hamiltonian-like constant of motion. Motivated by their study, we identify an analogous first integral of eq. (2.7):

$$H_0(t) := \frac{\gamma}{2 \langle u \rangle} z_0^2 + g(\theta_0) \quad (3.1)$$

[†] The mapping $\theta \mapsto \theta + \pi$ transforms $\langle u \rangle < 0$ into the positive case.

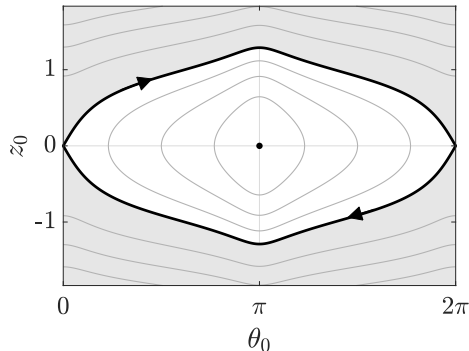


Figure 2: Phase portrait of motion on the intermediate timescale τ . Solutions of eq. (3.1) are closed orbits in the z_0 - θ_0 plane for constant H_0 , symmetric in both $z_0 = 0$ and $\theta_0 = \pi$. Solutions in the shaded region, where $H_0 > g(0)$, do not cross $z_0 = 0$, corresponding to tumbling motion and monotonic evolution of θ_0 . Trajectories with $H_0 < g(0)$ instead exhibit swinging motion, with θ_0 oscillating between two values. The black contour $H_0 = g(0)$ separates these regimes, with the direction of motion in the phase plane indicated by arrowheads, recalling that $\gamma \geq 0$. The point $(z_0, \theta_0) = (0, \pi)$ corresponds to rheotaxis, with $H_0 = g(\pi)$.

for $H_0(t) \in [g(\pi), \infty)$, where, for $\langle B \rangle \in (-1, 1)$,

$$g(\theta_0) := \frac{\operatorname{arctanh}\left(\sqrt{\frac{2\langle B \rangle}{1+\langle B \rangle}} \cos \theta_0\right)}{\sqrt{2\langle B \rangle(1+\langle B \rangle)}}, \quad g'(\theta_0) = -\frac{\sin \theta_0}{1-\langle B \rangle \cos 2\theta_0}, \quad (3.2)$$

taking the appropriate limits and branches where required. As $H_0(t)$ is effectively a constant of motion over the intermediate timescale τ , eq. (3.1) demonstrates that solutions to eq. (2.7) are closed orbits in z_0 - θ_0 phase space over this timescale, with θ_0 appropriately understood to be taken modulo 2π . We illustrate this phase space in fig. 2, equivalent to the plot of Zöttl & Stark (2013, Fig. 2b). In particular, it is helpful to emphasise the two distinct behavioural regimes on this timescale: (1) endless *tumbling*, where the swimmer does not cross $z_0 = 0$ and θ_0 varies monotonically, and (2) periodic *swinging*, where the swimmer repeatedly crosses the midline of the flow and θ_0 oscillates between two values, $\theta_0 \in [\theta_{\min}, \theta_{\max}]$, readily computed from eq. (3.1). The separating trajectory passes through $(z_0, \theta_0) = (0, 0)$ and corresponds to $H_0 = g(0)$. Here, $H_0 > g(0)$ corresponds to tumbling, shaded grey in fig. 2, and $H_0 < g(0)$ corresponds to swinging. Of note, the period of these dynamics over the intermediate timescale, which we denote by P_τ , depends non-trivially on H_0 .

We can identify these dynamics with those reported both numerically and experimentally by Omori *et al.* (2022). In particular, as $H_0(t)$ approaches its minimum of $g(\pi)$, the trajectory in the phase space approaches a single point, $(z_0, \theta_0) = (0, \pi)$, corresponding to a swimmer that is directed upstream on the midline of the flow. This is precisely the so-called *rheotactic* behaviour observed by Omori *et al.* (2022), which they noted as the long-time behaviour of eq. (1.1) for particular definitions of $u(T)$ and $B(T)$, corresponding also to the experimentally determined behaviours of *Chlamydomonas* in channel flow. This agreement suggests that the long-time dynamics of the full system may be captured by the evolution of the Hamiltonian-like quantity $H_0(t)$.

In order to examine this evolution, we consider the dynamics of the following

Hamiltonian-like expression,

$$H(t) := \frac{\gamma}{2\langle u \rangle} z^2 + g(\theta). \quad (3.3)$$

Taking the proper time derivative of eq. (3.3) and inserting eq. (2.1) yields

$$\frac{dH}{dt} = \gamma \omega^{1/2} z \sin \theta \left[\frac{u(T)}{\langle u \rangle} - \frac{1 - B(T) \cos 2\theta}{1 - \langle B \rangle \cos 2\theta} \right]. \quad (3.4)$$

Transforming the time derivative following eq. (2.2), we then insert our expansions of z and θ into eq. (3.4), noting that H is equal to H_0 at leading order. Expanding $H \sim H_0 + \omega^{-1/2} H_1 + \omega^{-1} H_2 + \dots$, the balance at $O(\omega)$ is simply $H_{0T} = 0$, so we deduce that $H_0 = H_0(\tau, t)$, as expected. At $O(\omega^{1/2})$, we have

$$H_{1T} + H_{0\tau} = \gamma z_0 \sin \theta_0 \left[\frac{u(T)}{\langle u \rangle} - \frac{1 - B(T) \cos 2\theta_0}{1 - \langle B \rangle \cos 2\theta_0} \right]. \quad (3.5)$$

Averaging over the fast timescale T , equivalent to applying the Fredholm solvability condition, we immediately see that the term in square brackets vanishes, so that $H_{0\tau} = 0$ and $H_0 = H_0(t)$ is also independent of τ , as expected.

Finally, we consider the $O(1)$ terms in eq. (3.4), which may be stated as

$$H_{2T} + H_{1\tau} + H_{0t} = h(T, \tau, t), \quad (3.6)$$

where

$$h(T, \tau, t) := \gamma (z_0 \theta_1 + z_1 \sin \theta_0) \left[\frac{u(T)}{\langle u \rangle} - \frac{1 - B(T) \cos 2\theta_0}{1 - \langle B \rangle \cos 2\theta_0} \right] - \frac{2\gamma z_0 \theta_1 \sin \theta_0 \sin 2\theta_0}{(1 - \langle B \rangle \cos 2\theta_0)^2} [B(T) - \langle B \rangle], \quad (3.7)$$

and we note that the expressions in the square brackets each average to zero over a period in T . Inserting our expressions for z_1 and θ_1 from eq. (2.9), we have

$$h(T, \tau, t) = \gamma (\sin^2 \theta_0 I_u(T) - \gamma z_0^2 \cos \theta_0 \cos 2\theta_0 I_B(T)) \left[\frac{u(T)}{\langle u \rangle} - \frac{1 - B(T) \cos 2\theta_0}{1 - \langle B \rangle \cos 2\theta_0} \right] + \frac{\gamma^2 z_0^2 \sin \theta_0 \sin 2\theta_0 \cos 2\theta_0}{(1 - \langle B \rangle \cos 2\theta_0)^2} I_B(T) (B(T) - \langle B \rangle) + [\cdot], \quad (3.8)$$

with $[\cdot]$ encompassing terms that have zero fast-timescale average, which here are those involving \bar{z}_1 and $\bar{\theta}_1$. It is also helpful to note that $2I_B(T)(B(T) - \langle B \rangle) = (I_B^2)_T$, so that $\langle I_B(B - \langle B \rangle) \rangle = 0$ by the periodicity of I_B . Hence, the entire second line of eq. (3.8) will vanish when averaged over a period in T . Averaging over T and noting the further relations $\langle I_B B \rangle = \langle I_B \langle B \rangle \rangle$, $\langle I_u u \rangle = \langle I_u \langle u \rangle \rangle$, and

$$(I_u I_B)_T = I_u(T)(B(T) - \langle B \rangle) + I_B(T)(u(T) - \langle u \rangle), \quad (3.9)$$

the fast-timescale average of h is simply

$$\langle h \rangle = \gamma \cos 2\theta_0 \left(\frac{\gamma}{\langle u \rangle} z_0^2 \cos \theta_0 + \frac{\sin^2 \theta_0}{1 - \langle B \rangle \cos 2\theta_0} \right) \underbrace{\langle I_u (B - \langle B \rangle) \rangle}_W, \quad (3.10)$$

where $W := \langle I_u (B - \langle B \rangle) \rangle$ is constant. Thus, averaging eq. (3.6) over a period in

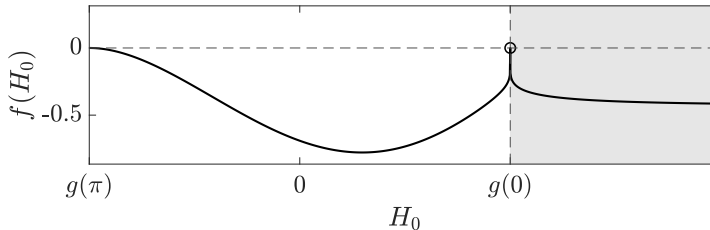


Figure 3: Exemplifying $f(H_0)$. We plot an example $f(H_0)$, as defined in eq. (3.12) and computed numerically, for a range of H_0 . The non-positivity of $f(H_0)$ is immediately evident, with $f \rightarrow 0$ from below as $H_0 \rightarrow g(\pi)$ or $H_0 \rightarrow g(0)$. As noted in the main text, f is undefined at $H_0 = g(0)$, which we indicate with a hollow circle, but this point is readily seen to be half stable in the context of the dynamical system of eq. (3.11), so has negligible impact on the dynamics in practice. Here, we have fixed $\gamma = 1$, $\langle u \rangle = 1$, and $\langle B \rangle = 0.5$. The shaded region corresponds to tumbling dynamics.

T and then over a period in τ^\dagger yields the long-time evolution equation

$$\frac{dH_0}{dt} = \gamma f(H_0)W, \quad (3.11)$$

where

$$f(H_0) := \frac{1}{P_\tau} \int_0^{P_\tau} \cos 2\theta_0 \left(\frac{\gamma}{\langle u \rangle} z_0^2 \cos \theta_0 + \frac{\sin^2 \theta_0}{1 - \langle B \rangle \cos 2\theta_0} \right) d\tau, \quad (3.12)$$

recalling that P_τ denotes the period of the oscillatory dynamics in τ and H_0 is independent of τ and T . Notably, the integrand of eq. (3.12) depends on the swimmer's speed and shape only via their fast-time averages $\langle u \rangle$ and $\langle B \rangle$. Therefore, all of the information encoding the dynamic variation of u and B about their mean is solely contained within the swimmer-dependent constant W . Of particular note, if either u or B is constant, then $W = 0$ and, hence, $dH_0/dt = 0$, so that there is no long-time drift of H_0 . This analytically verifies the numerical observations of Omori *et al.* (2022), who concluded that oscillations in both swimmer speed and shape were required to modify long-time behaviour.

Having reduced the dynamics to the one-dimensional autonomous dynamical system of eq. (3.11), notably independent of ω , it remains to understand $f(H_0)$, the average of a particular function of z_0 and θ_0 over a period in τ , which we illustrate in fig. 3. In appendix A, we analytically demonstrate that $f(H_0) \leq 0$ for all H_0 , in agreement with fig. 3. Hence, the sign of eq. (3.11) is determined by W , which depends only on the dynamics of u and B over a single oscillation. Strictly, there is a higher-order problem to be solved close to $H_0 = g(0)$, evidenced by the cusp-like profile in fig. 3, with $P_\tau \rightarrow \infty$ and $f(H_0) \rightarrow 0$ as $H_0 \rightarrow g(0)$. However, noting that $f(H_0) < 0$ either side of $H_0 = g(0)$, this point is half stable in the context of eq. (3.11) (Strogatz 2018), so that it is unstable in practice and does not materially impact on the evolving dynamics.

Thus, the fixed point at $H_0 = g(\pi)$, corresponding to the rheotactic configuration $(z_0, \theta_0) = (0, \pi)$, is globally stable if $W > 0$ and unstable if $W < 0$. Hence,

[†] Here, noting that H_0 is independent of τ , we can naively average over a single oscillation in τ , despite the t -dependence of P_τ , which would otherwise require the method of Kuzmak (1959).

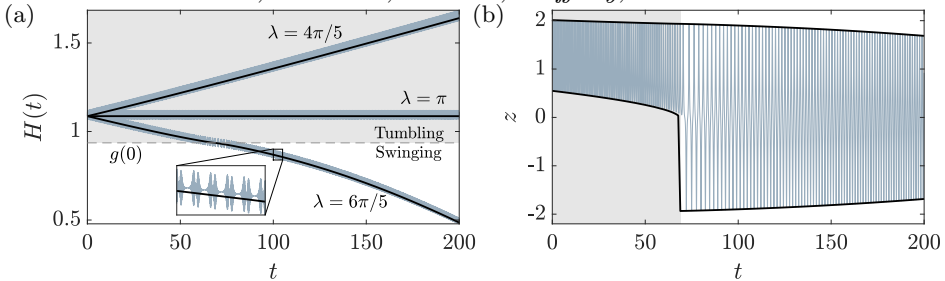


Figure 4: Numerical validation. (a) The value of H , as computed from the full numerical solution of eq. (2.1) and the approximation of eq. (3.11), shown as blue and black curves, respectively, for three phase shifts $\lambda \in \{4\pi/5, \pi, 6\pi/5\}$. Small, rapid oscillations in the full numerical solution are visible in the inset. (b) The asymptotically predicted bounds of z oscillations for $\lambda = 6\pi/5$ are shown as black curves, with the rapidly oscillating full solution shown in blue, highlighting excellent agreement even when the full solution transitions from tumbling dynamics towards rheotactic behaviour. Here, we have taken $(\alpha, \beta, \delta, \mu) = (1, 0.5, 0.32, 0.3)$ and $\lambda \in \{4\pi/5, \pi, 6\pi/5\}$ in the sinusoidal model of Omori *et al.* (2022), fixing $\gamma = 1$, $\omega = 50$, and $(z, \theta) = (1, \pi/4)$ initially. The shaded regions correspond to tumbling dynamics.

rheotaxis is the globally emergent behaviour at leading order if $W > 0$, whilst endless tumbling arises if $W < 0$.

4. Summary and conclusions

Our analysis allows us to characterise the long-time behaviour of a swimmer in Poiseuille flow via the computation of a simple quantity, W , defined in eq. (3.10) and dependent only on the dynamics of the speed u and the shape parameter B of the swimmer over a single oscillation. In particular, we find that the long-time behaviours take one of three possible forms, given in terms of the leading-order Hamiltonian-like quantity H_0 of eq. (3.1): (1) endless tumbling at increasing distance from the midline of the flow ($H_0 \rightarrow \infty$); (2) preserved initial behaviour of the swimmer ($H_0 = H_0(0)$); (3) convergence to upstream rheotaxis, where the swimmer is situated at the midline of the flow ($H_0 \rightarrow g(\pi)$). We find that the drift towards these long-time regimes is caused by the delicate higher-order interactions in the system. Specifically, the nonlinear interaction between the small $O(\omega^{-1/2})$ variations from the leading-order system over the fast timescale $t = O(\omega)$ gives rise to the significant $O(1)$ effect over the slow timescale $t = O(1)$.

In the context of Omori *et al.*, where $u(T) = \alpha + \beta \sin(2\pi T)$ and $B(T) = \delta + \mu \sin(2\pi T + \lambda)$, we note that in-phase oscillations with $\lambda \in \{n\pi | n \in \mathbb{Z}\}$ immediately lead to $W = 0$, corresponding to case (2) above. Any other values of λ lead to $W \neq 0$ (with maximal magnitude for $\lambda \in \{\pi/2 + n\pi | n \in \mathbb{Z}\}$) and long-term evolution of the swimmer behaviour. Notably, shifting λ by π results in a precise reversal of the sign of W and a corresponding reversal of the sign of dH_0/dt . Hence, this shift in phase will precisely flip the fate of the swimmer, with rheotaxis being replaced by tumbling, or vice versa. Concretely, if $\beta\mu > 0$, then $\lambda \in (0, \pi)$ results in tumbling, whilst $\lambda \in (\pi, 2\pi)$ gives rise to rheotaxis. Further, our analysis predicts that swimmers having either u or B constant will not undergo a similar drift over $t = O(1)$ at leading order. In particular, this highlights that rigid externally driven swimmers and Janus particles, associated

with constant B , would differ fundamentally in their long-time behaviour from shape-changing swimmers with dynamically varying B .

In support of our asymptotic analysis, we present three numerical examples in fig. 4, approximating $f(H_0)$ with quadrature using the easily obtained numerical solution of the simple ODE system of eq. (2.7) in τ for fixed $H_0(t)$. In fig. 4a, we compare the asymptotic and full numerical solutions through the evolution of H , adopting the sinusoidal model of Omori *et al.* (2022) and demonstrating excellent agreement between the solutions. This numerical validation spans the distinct dynamical regimes of tumbling and swinging, with different values of the phase shift λ giving rise to distinct behaviours from otherwise identical initial conditions. Figure 4b captures a transition between behaviours, as observed by Omori *et al.* (2022) for $\lambda = 6\pi/5$, where we have predicted the bounds of z oscillations by combining the solution of eq. (3.11) with eq. (3.1) evaluated at $\theta_0 = \theta_{\min}$ and $\theta_0 = \pi$. We anticipate that similar calculations may be used to predict collisions between swimmers and channel boundaries in related experimental set-ups, though theoretical consideration of boundary effects in future work is warranted and may complicate analysis. A promising direction for such an exploration is the augmentation of the model of Zöttl & Stark (2012) with the effects of an oscillatory swimming speed and swimmer shape, equivalent to extending the studied model of Omori *et al.* (2022) to a confined geometry.

More generally, the study of long-time swimmer dynamics in other scenarios, such as extensional flows, merits further investigation via multiscale analysis, with the behaviours of microswimmers in flow having been the subject of extensive research interest since the early 20th century, as summarised by Bretherton & Rothschild (1961). Recent examples of this include, but are not limited to, the works of Marcos *et al.* (2012); Miki & Clapham (2013) and Uspal *et al.* (2015), which consider the rheotaxis of spermatozoa, bacteria, and active particles, respectively. The study of microswimmers in flow has also recently been considered in the context of theoretical control and guidance (Moreau & Ishimoto 2021; Moreau *et al.* 2021; Walker *et al.* 2018), further motivating the development of our understanding of the potentially subtle interactions between swimmer shape, swimming speed, and background flows.

In summary, an asymptotic (three-timescale) multiple-scale analysis of the swimming model of Omori *et al.* (2022) has revealed a trichotomy of startlingly simple long-time behaviours, determined only by a single swimmer-specific constant of motion that may be readily computed a priori. This analysis, which complements the earlier works of Zöttl & Stark (2012, 2014) and Junot *et al.* (2019), confirms the numerical predictions of Omori *et al.* (2022), in agreement with their experimental observations of *Chlamydomonas*, and formally identifies the interacting oscillatory effects needed to elicit the eventual behaviours of endless tumbling and upstream rheotaxis in this model of swimming.

B.J.W. is supported by the Royal Commission for the Exhibition of 1851. K.I. acknowledges JSPS-KAKENHI for Young Researchers (Grant No. 18K13456), JSPS-KAKENHI for Transformative Research Areas (Grant No. 21H05309) and JST, PRESTO, Japan (Grant No. JPMJPR1921). C.M. is supported by the Research Institute for Mathematical Sciences, an International Joint Usage/Research Center located at Kyoto University. M.P.D. is supported by the UK Engineering and Physical Sciences Research Council [Grant No. EP/W032317/1].

The computer code used in this study is available at <https://gitlab.com/bjwalker/emergent-rheotaxis-in-Poiseuille-flow>.

Declaration of Interests. The authors report no conflict of interest.

Appendix A. Deducing the sign of $f(H_0)$

Consider the integrand of eq. (3.12). Recalling the evolution equations of z_0 and θ_0 on the intermediate timescale, given in eq. (2.7), this can be written as

$$\frac{\cos 2\theta_0}{\langle u \rangle (1 - \langle B \rangle \cos 2\theta_0)} (z_0 \sin \theta_0)_\tau.$$

Integrating by parts then yields

$$P_\tau f(H_0) = \int_0^{P_\tau} \frac{2z_0 \sin \theta_0 \sin 2\theta_0}{\langle u \rangle (1 - \langle B \rangle \cos 2\theta_0)^2} \theta_{0\tau} d\tau = \int \frac{2z_0 \sin \theta_0 \sin 2\theta_0}{\langle u \rangle (1 - \langle B \rangle \cos 2\theta_0)^2} d\theta_0, \quad (\text{A } 1)$$

with boundary terms vanishing due to periodicity. With reference to the phase diagram of fig. 2, we note that we need only integrate in θ_0 from its minimum attained value up to π , with both the integrand and the phase-space trajectory being symmetric about both $\theta_0 = \pi$ and $z_0 = 0$. This corresponds to integrating over the branch of the trajectory in the upper-left quadrant of fig. 2, with the true value of $P_\tau f(H_0)$ then being recovered by appropriate multiplication by two or four, depending on whether the trajectory is one of tumbling or swinging. Hence, we consider the integral only over the range $\theta_0 \in [\theta_{\min}, \pi]$, where $\theta_{\min} \in [0, \pi]$ is the minimum value attained by θ_0 over an orbit, as specified solely by $H_0(t)$.

In the upper-left quadrant of the phase plane, z_0 is a non-negative increasing function of θ_0 , evident from eq. (2.7a) and eq. (3.1). In particular, $z_0(\theta_0 + \pi/2) \geq z_0(\pi/2)$ for $\theta_0 \in [0, \pi/2]$. Further, the remaining combination of trigonometric terms in the integrand, denoted by $I(\theta_0)$ for brevity, satisfies $I(\theta_0) \geq 0$ and $I(\theta_0 + \pi/2) = -I(\theta_0)$ for $\theta_0 \in [0, \pi/2]$. Hence, the integral is trivially negative for $\theta_{\min} \in [\pi/2, \pi]$, whilst for $\theta_{\min} \in [0, \pi/2]$ we have

$$\begin{aligned} \int_{\theta_{\min}}^{\pi} z_0(\theta_0) I(\theta_0) d\theta_0 &= \int_{\theta_{\min}}^{\pi/2} z_0(\theta_0) I(\theta_0) d\theta_0 + \int_{\pi/2}^{\pi} z_0(\theta_0) I(\theta_0) d\theta_0 \\ &\leq \int_0^{\pi/2} z_0(\pi/2) I(\theta_0) d\theta_0 + \int_0^{\pi/2} z_0(\theta_0 + \pi/2) I(\theta_0 + \pi/2) d\theta_0 \\ &= \int_0^{\pi/2} [z_0(\pi/2) - z_0(\theta_0 + \pi/2)] I(\theta_0) d\theta_0 \leq 0. \end{aligned} \quad (\text{A } 2)$$

Hence, $P_\tau f(H_0) \leq 0$, so that $f(H_0) \leq 0$ for all H_0 . In particular, this equality is strict unless $H_0 = g(\pi)$ or $H_0 = g(0)$, which correspond to the degenerate rheotactic trajectory $(z_0, \theta_0) = (0, \pi)$ and the separating trajectory that lies between tumbling and swinging behaviours in fig. 2. As discussed in the main text, the case with $H_0 = g(0)$ requires the consideration of a higher-order problem, though has negligible impact on the dynamics in practice.

REFERENCES

- BENDER, C. M. & ORSZAG, S. A. 1999 *Advanced Mathematical Methods for Scientists and Engineers I*. New York, NY: Springer New York.

- BRETHERTON, F. P. 1962 The motion of rigid particles in a shear flow at low Reynolds number. *Journal of Fluid Mechanics* **14** (2), 284–304.
- BRETHERTON, F. P. & ROTHSCHILD 1961 Rheotaxis of Spermatozoa. *Proceedings of the Royal Society B: Biological Sciences* **153** (953), 490–502.
- GAFFNEY, E. A., DALWADI, M. P., MOREAU, C., ISHIMOTO, K. & WALKER, B. J. 2022 Canonical orbits for rapidly deforming planar microswimmers in shear flow. *Physical Review Fluids* **7** (2), L022101.
- GUASTO, J. S., RUSCONI, R. & STOCKER, R. 2012 Fluid mechanics of planktonic microorganisms. *Annual Review of Fluid Mechanics* **44** (1), 373–400.
- JUNOT, G., FIGUEROA-MORALES, N., DARNIGE, T., LINDNER, A., SOTO, R., AURADOU, H. & CLÉMENT, E. 2019 Swimming bacteria in Poiseuille flow: The quest for active Bretherton-Jeffery trajectories. *Epl* **126** (4).
- KIM, S. & KARRILA, S. J. 2005 *Microhydrodynamics: Principles and Selected Applications*. Dover Publications.
- KUZMAK, G. 1959 Asymptotic solutions of nonlinear second order differential equations with variable coefficients. *Journal of Applied Mathematics and Mechanics* **23** (3), 730–744.
- MA, K., PUJARA, N. & THIFFEAULT, J.-L. 2022 Reaching for the surface: Spheroidal microswimmers in surface gravity waves. *Physical Review Fluids* **7** (1), 014310.
- MARCOS, FU, H. C., POWERS, T. R. & STOCKER, R. 2012 Bacterial rheotaxis. *Proceedings of the National Academy of Sciences* **109** (13), 4780–4785.
- MIKI, K. & CLAPHAM, D. E. 2013 Rheotaxis Guides Mammalian Sperm. *Current Biology* **23** (6), 443–452.
- MOREAU, C. & ISHIMOTO, K. 2021 Driving a microswimmer with wall-induced flow. *Micromachines* **12** (9).
- MOREAU, C., ISHIMOTO, K., GAFFNEY, E. A. & WALKER, B. J. 2021 Control and controllability of microswimmers by a shearing flow. *Royal Society Open Science* **8** (8), 211141.
- OMORI, T., KIKUCHI, K., SCHMITZ, M., PAVLOVIC, M., CHUANG, C. H. & ISHIKAWA, T. 2022 Rheotaxis and migration of an unsteady microswimmer. *Journal of Fluid Mechanics* **930**, 1–17.
- STROGATZ, S. H. 2018 *Nonlinear Dynamics and Chaos*. CRC Press.
- USPAL, W. E., POPESCU, M. N., DIETRICH, S. & TASINKEVYCH, M. 2015 Rheotaxis of spherical active particles near a planar wall. *Soft Matter* **11** (33), 6613–6632.
- WALKER, B. J., ISHIMOTO, K., GAFFNEY, E. A., MOREAU, C. & DALWADI, M. P. 2022 Effects of rapid yawing on simple swimmer models and planar Jeffery’s orbits. *Physical Review Fluids* **7** (2), 023101.
- WALKER, B. J., ISHIMOTO, K., WHEELER, R. J. & GAFFNEY, E. A. 2018 Response of monoflagellate pullers to a shearing flow: A simulation study of microswimmer guidance. *Physical Review E* **98** (6), 063111.
- ZÖTTL, A. & STARK, H. 2012 Nonlinear Dynamics of a Microswimmer in Poiseuille Flow. *Physical Review Letters* **108** (21), 218104.
- ZÖTTL, A. & STARK, H. 2013 Periodic and quasiperiodic motion of an elongated microswimmer in Poiseuille flow. *The European Physical Journal E* **36** (1), 4.
- ZÖTTL, A. & STARK, H. 2014 Hydrodynamics Determines Collective Motion and Phase Behavior of Active Colloids in Quasi-Two-Dimensional Confinement. *Physical Review Letters* **112** (11), 118101.